JST: Smart Systems and Devices
Volume 34, Issue 1, January 2024, 031-041

Study of the Dynamics of Automated Guided Vehicle Using Mecanum Omnidirectional Wheel

Tong Xuan Loc, Truong Dang Viet Thang, Ho Huu Hai*
Hanoi University of Science and Technology, Ha Noi, Vietnam
**Corresponding author email: hai.hohuu@hust.edu.vn*

Abstract

The paper presents the result of the dynamics simulation of automated guided vehicles (AGVs) using four Mecanum omnidirectional wheels when the tilt angle of each wheel's roller is changed. Mecanum omnidirectional wheels have the ability to work flexibly, but operators are generally concerned about the vehicle's efficiency issues. The performance of the wheel significantly influences the extensive application range of the vehicle. The method of modeling automated guided vehicles and Mecanum wheels is applied in order to build its kinematic model and dynamic model with omnidirectional wheels when the roller's angle of incline is changed. Based on Lagrange equation of 2nd type, the equation of motion of the vehicle is established in accordance with the actual situation that the vehicle is being applied. The rolling friction coefficient and the adhesive coefficient of Mecanum wheels were measured experimentally on different road surfaces, including concrete, wood, brick, and stone. The study's findings successfully address efficiency challenges in vehicles using omnidirectional wheels when varying the incline angle of each roller and applying fuzzy logic for trajectory control in autonomous vehicles.

Keywords: Automated guided vehicles (AGVs), fuzzy logic control, Lagrange equation of 2nd type, mecanum omnidirectional wheel

1. Introduction

Navigating and moving a vehicle in a tight, confined space is a complicated and challenging problem. One solution to this problem is the development of omnidirectional wheels, which can move directly in many different directions.

The omnidirectional wheel has a wide range of applications in many fields, including industry, public security, medical as well as scientific research, etc. This wheel type is often applied in robots requiring flexible movement without a steering system. Automated guided vehicles (AGVs) with four Mecanum wheels are the most widely involved in the industry for transporting heavy equipment, such as the MC Drive TP2000 robot used to transport Airbus aircraft parts.

In Vietnam, many articles discuss research on AGVs employing Mecanum wheels, but these articles primarily emphasize the design of omnidirectional wheels and the control of AGV motion trajectories. In 2012, Tran Dinh Phuc [1] pointed out that passing through a narrow space is difficult and complicated for forklifts. Thus, the author designed the omnidirectional wheel applied in this type of forklift. With the required parameters, the author calculated the profile of the Mecanum wheel used in forklifts. After designing, the accuracy of the wheel profile was assessed. The dissertation researched and formulated the design path of Mecanum roller profile calculation, compared the advantages and disadvantages of roller profile design methods, designed and manufactured Mecanum wheels for forklifts, measured and evaluated roller profile accuracy, thereby drew conclusions about the causes of subtype profile errors of rollers. However, the evaluation of the wheel performance after designing is not considered.

In 2017, Vo Phong Thien [2] selected the design options and analyzed the kinematic equations of an automated guided robot model in a factory. As a result, the author designed a robot model, established electrical systems, sensors, and control, completed the connection of power module, conducted an experiment using sensors, control motor and found the error of traction coefficient for the robot. Experimental results show that the robot has performed the task of moving in a warehouse. The thesis has completed the set objectives, but some limitations remain. The robot is unstable during movement due to numerous uncontrollable external environmental influences. Additionally, the mechanical model lacks guaranteed motor shaft concentricity. Consequently, the robot moving in a straight path necessitates further adjustments through programming. The model only meets the demands of goods transportation and movement within the factory.

Numerous comprehensive published articles have explored research pertaining to AGVs utilizing

ISSN: 2734-9373
https://doi.org/10.51316/jst.171.ssad.2024.34.1.5
Received: October 9, 2023; accepted: December 1, 2023

Mecanum wheels in-depth. In 2011, Adascalitei F. *et al*. [3] discussed the innovative applications of Mecanum wheels in mobility and industry. The most common configurations of a Mecanum wheel, as well as its advantages and disadvantages in terms of wheel arrangement solutions to improve and optimize the vehicle's maneuverability, have been presented in this thesis. Many applications of Mecanum wheels have been analyzed in the article, such as self-propelled robots, AGVs in factories, wheelchairs, and scout cars.

In 2014, Felix Becker [4] and colleagues proposed a different approach to simulate vehicle dynamics using Mecanum wheels. The authors analyzed the kinematics and then used the Lagrange equation to establish the dynamic equation for self-propelled vehicles using omnidirectional wheels. This resulted from conducting dynamic simulations of the vehicle using Mecanum wheels with length and width parameters differing for various vehicles. The results from the theoretical and experimental simulations are nearly identical; however, there are still some errors. The primary reason for these errors is that the author's team likely overlooked the rolling friction component when setting up the vehicle's equation of motion.

In 2017, Z. Hendzel and L. Rykała [5] established a dynamic model of a Mecanum wheel robot using Lagrange equation of 2nd type, thereby simulating the motion of Mecanum wheels. The authors referred to [4] in this article and incorporated the rolling friction component into the dynamics equation. However, the coefficient of rolling friction the authors took is a constant. In reality, it changes depending on the speed of the vehicle. From the simulation results, the direction of movement of the robot in simulation and reality is quite similar, but there are still certain errors, and an evaluation of the wheel's performance is not available.

In 2016, Matthieu Lamy [6] developed a mechanical model for the AGV, including the Mecanum chassis, chassis, and wheels. The vehicle must be compact yet capable of carrying heavy, bulky objects while maintaining flexibility. The author analyzed and chose to use Mecanum wheels to meet this requirement. The author designed detailed models of Mecanum wheels and the chassis, then simulated and tested the durability of the components. Based on the simulation results, the author evaluated the material selection and proposed a complete model at a more affordable price.

In 2019, the author P.L. Sarode and colleagues [7] designed and manufactured omnidirectional wheels for forklifts. They began by selecting materials for the multi-directional wheels based on specified requirements and then used Catia software to design and simulate both the wheels and chassis. After extensive calculations and analysis, a forklift model with multi-directional wheels was successfully built, utilizing appropriate materials for each component to meet cost and durability requirements.

In 2015, referring to [8] by author Nishant Sonawane, the adhesion coefficient of omnidirectional wheels was determined through experiments conducted under various conditions. The author utilized different devices, including a tribometer and force sensor, to obtain adhesion coefficient results on surfaces such as wood, paint, concrete, and others. However, the article lacks clarity regarding the adhesion coefficient results.

In 2019, Zeidis, Igor, and Zimmermann, Klaus [9] developed a kinetic and dynamic model for vehicles equipped with omnidirectional wheels. They established two methods for determining the equations of motion for such vehicles and conducted simulations of their dynamics. However, the author overlooked the rolling resistance component during the analysis of forces acting on the vehicle. This omission led to the simulation results showing the vehicle's speed approaching infinity. Rolling friction force during vehicle movement varies constantly, depending on factors such as vehicle velocity, tire material, tire structure, tire pressure, tire temperature, torque applied to the wheel, road surface material and condition, and vehicle speed.

The rolling friction coefficient of the Mecanum omnidirectional wheel has not been mentioned in any article. With the aim of studying, autonomous vehicles using omnidirectional wheels, this study presents a method for establishing the equations of motion for autonomous vehicles equipped with Mecanum omnidirectional wheels. It calculates the rolling resistance coefficient and adhesive coefficient of these wheels, allowing for the simulation and evaluation of wheel performance.

This paper derives kinetic and dynamic models and the equation of motion from [9], considering various parameters of the roller's angle of incline and simulating the vehicle's movement under the influence of rolling resistance.

1.1. Mathematical Model of AGV Using Omnidirectional Wheels

In reference to [9], this article builds upon the kinematic and dynamic equations while extending them to account for variations in the incline angle of each roller.

The motion of AGV is a complex motion including three translational travels in the x, y, z-axis and three angular motions α, β, ψ. The fixed coordinate system G ($OXYZ$) was established, and the body coordinate system B ($Cxyz$) was also used to characterize this motion. The vehicle is considered to always be in contact with the plane, and the wheels are arranged in parallel on the two axles. The AGV has

mass m_s, center of mass C lies on the longitudinal axis of symmetry of the vehicle. The distance from the center of mass C of the car to each axle is ρ, and the distance between the centers of the wheels is $2l$. ψ is the angle between the rotating body coordinate system B ($Cxyz$) and the fixed coordinate system G ($OXYZ$) (Fig. 1). The rotating angle of the wheels relative to the axis perpendicular to the plane of the corresponding wheels and passing through their centers is φ_i, the corresponding torques of the wheels are M_i (i = 1,…,4).

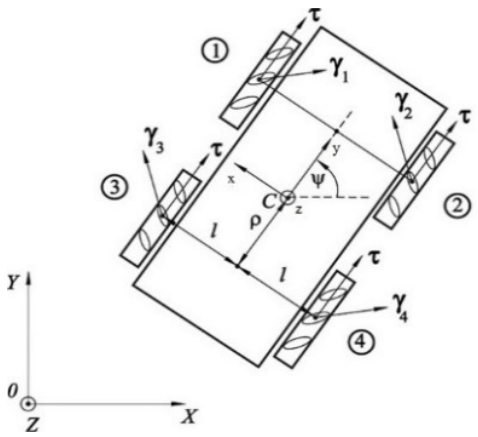

Fig. 1. AGV vehicle using omnidirectional wheels

The omnidirectional wheel has rollers with fixed axles on the outer rim, where the axis of each roller forms the same angle δ ($0° < \delta < 90°$). Each roller can rotate freely around its axis, and the wheel can roll on the rollers. Considering the model of an omnidirectional wheel with a radius R, the velocity V_P of the point of contact P on the disc with the supporting plane is orthogonal to the axis of the roller (Fig. 2). The rollers are fastened to the shafts centered at the wheel's circumference. With these assumptions, the Mecanum wheel model, in which the rollers are infinitely small, can be used for research and calculations.

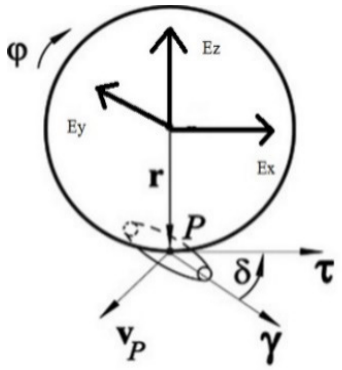

Fig. 2. Mecanum wheel model

where γ is the unit vector of the roller axis. The wheels move without slipping when:

$$\overrightarrow{V_P}.\vec{\gamma} = 0 \quad (1)$$

Based on the Euler equation, if $\overrightarrow{V_K}$ is the speed at the center of the wheel, then:

$$\overrightarrow{V_P} = \overrightarrow{V_K} + \vec{\omega} \times \vec{R} \quad (2)$$

where:

$\vec{\omega}$: wheel angular velocity vector

$\vec{R}$: wheel radius vector, $\vec{R} = -\overrightarrow{KP}.\overrightarrow{E_z}$

φ: wheel rotation angle

Therefore (1) can be written as:

$$\left(\overrightarrow{V_K} - \vec{R} \times \dot{\varphi}.\vec{\tau}\right).\vec{\gamma} = 0 \quad (3)$$

where $\vec{\tau}$ is unit tangent vector to the wheel at the point of contact.

From the expression (3) we have:

$$\overrightarrow{V_K}.\vec{\gamma} = \vec{R}.\dot{\varphi}.cos\delta \quad (4)$$

where δ is the angle between wheel rollers and wheel axle

1.2. Kinematic Equations

V_C is the velocity of the vehicle's center of mass and $r_i = \overrightarrow{CK_i}$

Velocity vector at the center of wheels:

$$\overrightarrow{V_{Ki}} = \overrightarrow{V_C} + \overrightarrow{\dot{\psi}} \times \vec{r_i} \ (i=1,...,4) \quad (5)$$

With $\dot{\vec{\psi}}$ being the angular velocity of the vehicle body, equation (4) can be written as:

$$\left(\overrightarrow{V_C} + \vec{\dot{\psi}} \times \vec{r_i}\right) \times \overrightarrow{\gamma_i} = R.\dot{\varphi}_i.cos\ \delta \quad (6)$$

$$<=> \overrightarrow{V_C}.\overrightarrow{\gamma_i} + (\vec{r_i} \times \overrightarrow{\gamma_i}) \times \vec{\dot{\psi}} = R.\dot{\varphi}_i.cos\ \delta$$

where $\overrightarrow{\gamma_i}$ is unit vector according to the roller axis of the corresponding wheel.

Consider the vehicle in the body coordinate system B ($Cxyz$) with the Cx axis being the horizontal symmetry axis, Cy being the longitudinal symmetry axis and the Cz axis perpendicular to the Cxy plane, equation (6) on the body coordinate system we have:

$$V_{Cx}.\gamma_{ix}. + V_{Cy}.\gamma_{iy} + (r_{iy}.\Gamma_{ix} - r_{ix}.\Gamma_{iy}).\dot{\Psi} = R.\dot{\varphi}_i.\cos\delta \quad (7)$$

where:

$\gamma_{1x} = \gamma_{4x} = \cos\delta$; $\gamma_{1y} = \gamma_{4y} = -\sin\delta$

$\gamma_{2x} = \gamma_{3x} = \cos\delta$; $\gamma_{2y} = \gamma_{3y} = \sin\delta$

$r_{1x} = r_{2x} = \rho$; $r_{1y} = r_{3y} = l$

$r_{3x} = r_{4x} = -\rho$; $r_{2y} = r_{4y} = -l$

Constraint equation (7) becomes:

$$\begin{cases} V_{Cx}.\cos\delta - V_{Cy}.\sin\delta - (\rho.\cos\delta + l.\sin\delta).\dot{\psi} = R.\dot{\varphi}_1.\cos\delta \\ V_{Cx}.\cos\delta + V_{Cy}.\sin\delta + (\rho.\cos\delta + l.\sin\delta).\dot{\psi} = R.\dot{\varphi}_2.\cos\delta \\ V_{Cx}.\cos\delta + V_{Cy}.\sin\delta - (\rho.\cos\delta + l.\sin\delta).\dot{\psi} = R.\dot{\varphi}_3.\cos\delta \\ V_{Cx}.\cos\delta - V_{Cy}.\sin\delta + (\rho.\cos\delta + l.\sin\delta).\dot{\psi} = R.\dot{\varphi}_4.\cos\delta \end{cases} \quad (8)$$

Four equations in (8) can be written equivalently as follows:

$$\begin{cases} V_{Cx} = \frac{R}{2}.(\dot{\varphi}_1 + \dot{\varphi}_2) \\ V_{Cy} = \frac{R.\cos\delta}{2.\sin\delta}.(\dot{\varphi}_3 - \dot{\varphi}_1) = \frac{R.\cot\delta}{2}.(\dot{\varphi}_3 - \dot{\varphi}_1) \\ \dot{\psi} = \frac{R}{2.(\rho.\cos\delta + l.\sin\delta).}.(\dot{\varphi}_2 - \dot{\varphi}_3).\cos\delta \\ \dot{\varphi}_1 + \dot{\varphi}_2 = \dot{\varphi}_3 + \dot{\varphi}_4 \end{cases} \quad (9)$$

Consider the fixed axis system *OXYZ*:

$$\begin{cases} \dot{x_c} = V_{Cx}.\cos\psi - V_{Cy}.\sin\psi \\ \dot{y_c} = V_{Cx}.\sin\psi + V_{Cy}.\cos\psi \end{cases} \quad (10)$$

From equation (9) the following equations can be inferred:

$$\begin{cases} \psi = \frac{R}{2.(\rho.\cos\delta + l.\sin\delta).}.(\dot{\varphi}_2 - \dot{\varphi}_3).\cos\delta + C_1 \\ \varphi_4 = \varphi_1 + \varphi_2 - \varphi_3 + C_2 \end{cases} \quad (11)$$

1.3. Equations of Motion of the Vehicle

AGVs is considered as a rectangular plane moving on the road surface, the system under consideration is determined by seven general coordinates: x_C, y_C, ψ, φ_1, φ_2, φ_3, φ_4. In this section, the dynamics of the solid-body model of the Mecanum car and wheels will be presented by starting from Newton's 2nd postulate, establishing the kinetic energy change theorems and the conservation of mechanical energy theorem, then applying Lagrange equation of 2nd type to build differential equations of motion of the mechanical system. For the mechanical system under consideration, the equations of Lagrange equation of 2nd type are given by:

$$\frac{d}{dt}\left(\frac{\partial T}{\partial \dot{\varphi}_s}\right) - \frac{\partial T}{\partial \varphi_s} = Q_s,\ s = 1,\ldots,4 \quad (12)$$

Kinetic energy T_0 of translational motion is:

$$T_0 = \frac{1}{2}(m_0 + 4m_1)\overrightarrow{v_c^2} \quad (13)$$

Kinetic energy T_1 of rotation is:

$$T_1 = \frac{1}{2}(J_0 + 4(J_2 + m_1(\rho^2 + l^2)))\dot{\psi}^2 + \frac{J_1}{2}(\dot{\varphi_1}^2 + \dot{\varphi_2}^2 + \dot{\varphi_3}^2 + \dot{\varphi_4}^2) \quad (14)$$

where:

J_0 is the moment of inertia of the object about the center of mass C

J_1 is the moment of inertia of the wheel about an axis perpendicular to the plane of the wheel and passing through its center of mass.

J_2 is the moment of inertia of the wheel about the vertical axis passing through the center of mass of the vehicle

The equation of the constraint kinematics of (8) is expressed by matrix form:

$$\dot{\boldsymbol{\varphi}} = \boldsymbol{J}\boldsymbol{V} \quad (15)$$

Here, the vector $\dot{\boldsymbol{\varphi}}$ is 4×1, the matrix $\boldsymbol{J}$ is 4×3 and the vector $\boldsymbol{V}$ is 3×1

$$\dot{\boldsymbol{\varphi}} = \begin{pmatrix} \dot{\varphi}_1.cos\delta \\ \dot{\varphi}_2.cos\delta \\ \dot{\varphi}_3.cos\delta \\ \dot{\varphi}_4.cos\delta \end{pmatrix}, \quad \boldsymbol{V} = \begin{pmatrix} V_{cx}.cos\delta \\ V_{cy}.cos\delta \\ (\rho.cos\delta + l.sin\delta).\dot{\psi} \end{pmatrix}, \quad \boldsymbol{J} = \frac{1}{R}\begin{pmatrix} 1 & -1 & -1 \\ 1 & 1 & 1 \\ 1 & 1 & -1 \\ 1 & -1 & 1 \end{pmatrix} \quad (16)$$

The $\mathbf{J^T}$ transpose matrix has the form:

$$\mathbf{J^T} = \frac{1}{R}\begin{pmatrix} 1 & 1 & 1 & 1 \\ -1 & 1 & 1 & -1 \\ -1 & 1 & -1 & 1 \end{pmatrix} \quad (17)$$

Multiplying the (15) by the displacement matrix $\boldsymbol{J^T}$, we get:

$$\boldsymbol{J^T}.\dot{\boldsymbol{\varphi}} = \boldsymbol{J^T}.\boldsymbol{J}.\boldsymbol{V} \quad (18)$$

The matrix $\boldsymbol{J^T}.\boldsymbol{J}$ has the corresponding inverse $(\boldsymbol{J^T}.\boldsymbol{J})^{-1}$. From the (18) we get:

$$\boldsymbol{V} = \boldsymbol{J^+}.\dot{\boldsymbol{\varphi}},\ \boldsymbol{J^+} = (\boldsymbol{J^T}.\boldsymbol{J})^{-1}.\boldsymbol{J^T} \quad (19)$$

The matrix $\boldsymbol{J^+}$ is the inverse of $\boldsymbol{J}$:

$$\boldsymbol{J^+} = \frac{R}{4}\begin{pmatrix} 1 & 1 & 1 & 1 \\ -1 & 1 & 1 & -1 \\ -1 & 1 & -1 & 1 \end{pmatrix} \quad (20)$$

Form the equations (15) – (21) we have:

$$\begin{cases} V_{cx} = \frac{R}{4}.(\dot{\varphi}_1 + \dot{\varphi}_2 + \dot{\varphi}_3 + \dot{\varphi}_4) \\ V_{cy} = \frac{R.cos\delta}{4.sin\delta}.(-\dot{\varphi}_1 + \dot{\varphi}_2 + \dot{\varphi}_3 - \dot{\varphi}_4) \\ \dot{\psi} = \frac{R.cos\delta}{4.(\rho.cos\delta + l.sin\delta)}.(-\dot{\varphi}_1 + \dot{\varphi}_2 - \dot{\varphi}_3 + \dot{\varphi}_4) \end{cases} \quad (21)$$

The equations (21), (13), (14) result in:

$$T= \frac{A}{2}.(\dot{\varphi_1}^2+\dot{\varphi_2}^2+\dot{\varphi_3}^2+\dot{\varphi_4}^2+ B.(\dot{\varphi_1}.\dot{\varphi_2}+\dot{\varphi_1}.\dot{\varphi_3}+\dot{\varphi_2}\dot{\varphi_4}+ \dot{\varphi_3}\dot{\varphi_4})-C.(\dot{\varphi_1}\dot{\varphi_2}-\dot{\varphi_1}\dot{\varphi_3}-\dot{\varphi_2}\dot{\varphi_4}+ \dot{\varphi_3}\varphi_4)+D.(\dot{\varphi_1}\dot{\varphi_4}+\dot{\varphi_2}\dot{\varphi_3}) \quad (22)$$

in which:

$$A= m_s.\frac{R^2}{16}\left(1+\frac{cos\delta^2}{sin\delta^2}\right)+\frac{J_c.R^2}{16.(\rho.cos\delta+l.sin\delta)^2}+J_1 \quad (23)$$

$$B = m_s.\frac{R^2}{16}(1-\frac{cos\delta^2}{sin\delta^2}).(\dot{\varphi_1}.\dot{\varphi_2}+\dot{\varphi_1}.\dot{\varphi_3}+\dot{\varphi_2}\dot{\varphi_4}+\dot{\varphi_3}\dot{\varphi_4}) \quad (24)$$

$$C = J_c.\frac{R^2}{16.(\rho.cos\delta+l.sin\delta)^2}.(-\dot{\varphi_1}.\dot{\varphi_2}+\dot{\varphi_1}.\dot{\varphi_3}+\dot{\varphi_2}\dot{\varphi_4}-\dot{\varphi_3}\dot{\varphi_4}) \quad (25)$$

$$D = m_s.\frac{R^2}{16}(\frac{1}{sin\delta^2}-\frac{J_c.R^2}{16.(\rho.cos\delta+l.sin\delta)^2} \quad (26)$$

The equation (22) is substituted into the (12):

$$\begin{cases} A.\ddot{\varphi_1}+B.(\ddot{\varphi_2}+\ddot{\varphi_3})-C.(\ddot{\varphi_2}-\ddot{\varphi_3})+D.\ddot{\varphi_4}=M_1-M_c \\ A.\ddot{\varphi_2}+B.(\ddot{\varphi_1}+\ddot{\varphi_4})-C.(\ddot{\varphi_1}-\ddot{\varphi_4})+D.\ddot{\varphi_3}=M_2-M_c \\ A.\ddot{\varphi_3}+B.(\ddot{\varphi_1}+\ddot{\varphi_4})+C.(\ddot{\varphi_1}-\ddot{\varphi_4})+D.\ddot{\varphi_2}=M_3-M_c \\ A.\ddot{\varphi_4}+B.(\ddot{\varphi_2}+\ddot{\varphi_3})+C.(\ddot{\varphi_2}-\ddot{\varphi_3})+D.\ddot{\varphi_1}=M_4-M_c \end{cases} \quad (27)$$

For $M_{s(t)}$, where s = 1…4 is given as a function of time, system of (27) can be easily integrated depending on the respective initial conditions. The projections of the velocity vectors V_{cx}, V_{cy} for the center of mass and the angular velocity of the body $\dot{\psi}$, are determined using constraint (21).

$$V_{cx} = \frac{R}{4.(A+D)}.\int_0^t(M_1+M_2+M_3+M_4-4M_c)\,d_t$$
$$V_{cy} = \frac{-R.cos\delta}{4.(A+D).sin\delta}.\int_0^t(M_1-M_2+M_3-M_4-4M_c)\,d_t \quad (28)$$
$$\dot{\psi} = \frac{-R.cos\delta}{4.(\rho.cos\delta+l.sin\delta).(A+2C-D)}.\int_0^t(M_1-M_2+M_3-M_4-4M_c)\,d_t$$

Thus, with the (10), (27) and (28), it is possible to determine the trajectory and speed of the AGV using the variables M_1, M_2, M_3 and M_4.

2. Experiments to Measure the Coefficient of Adhesion and Rolling Friction of Mecanum Wheels

2.1. Experiment to Measure Adhesion Coefficient of Mecanum Wheels by Dropping Method on Gradient Plane

2.1.1. Measurement method

The coefficient of adhesion is a dimensionless quantity, and its value is equal to the ratio of the adhesive force (P_ϑ) of the wheel and the normal reaction from the road surface (G_ϑ) acting on tire contact patch. In the general case, the coefficient of adhesion, denoted ϑ, is determined as below:

$$\vartheta = \frac{P_\vartheta}{G_\vartheta} \quad (29)$$

When dropped on a declined platform without air drag resistance, the vehicle is under the influence of the inertia and gravity forces.

If the slope angle is gradually increased, the inertia force of the vehicle augments steadily. During the vehicle starts rolling, the inertia force is greater than or equal to the adhesive force $F_{qt} \geq P_\vartheta$.

in which:

$$F_{qt} = P.\sin\alpha$$
$$G_\varphi = P.\cos\alpha \quad (30)$$

α: slope angle when the vihicle starts sliding

When the vehicle is placed on a slope, and the angle of inclination of the gradient plane is gradually increased, the coefficient of adhesion is determined entirely by the following formula:

$$\vartheta = \frac{P_\vartheta}{G_\vartheta} = \frac{F_{qt}}{G_\vartheta} = \frac{P.sin\,\alpha}{P.cos\,\alpha} = tan\,\alpha \quad (31)$$

Thus, the exact adhesion coefficient of the vehicle will be determined if the sloping declination is clarified when the vehicle starts sliding.

2.1.2. Experiment equipment

Experimental equipment includes 4 parts as following:

- Experiment AGV is All-Wheel Drive vehicle which uses mecanum wheels, each wheel is equipped with 1 motor (Fig. 3).

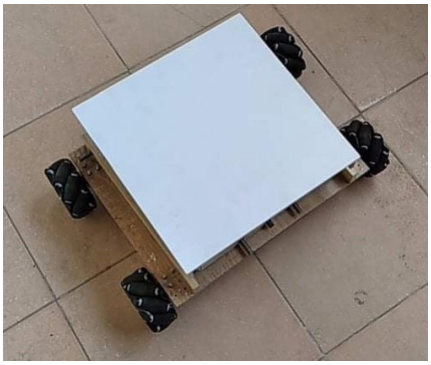

Fig. 3. Experiment AGV

Table 1. Specifications of experiment AGV

Specifications	Symbol	Value	Unit
Vehicle mass	m_s	6,6	Kg
Wheel mass	m_i	0.4	Kg
Length	-	0.8	m
Width	-	0.6	m
Height	-	0.3	m
Load on each wheel	P_i	16.17	N

- Mecanum wheel: the wheel has a body material of plastic, the material of the auxiliary roller is rubber. Wheel diameter and width are 0.1 x 0.04 (m), respectively. The wheel has 9 rollers arranged around it, the axis of each roller forms the same angle 45^0. Roller length is 0.05 m.

- Wooden plane: a flat wooden board with dimensions of length, width, and height, respectively, as follows: 1 x 1 x 0.1 (m).

- Degree ruler: Degree ruler with the smallest measuring increment of 0.5 degrees.

The specific parameters of the vehicle are presented in the following Table 1.

2.1.3. Experiment procedure

Perform the experiment following the steps below:

Step 1: Determine the weight of the vehicle.

Step 2: Lock all wheels and put the vehicle on a wooden surface.

Step 3: Slip one side of the wooden board gradually to increase the incline angle between the wooden board and the road surface (angle α). When the vehicle starts moving, record the incline angle α.

Step 4: Conduct 5 times to record the results in the data table.

2.1.4. Experiment results

The experiment was conducted on the wooden plane, and the following results were obtained as described in Table 2.

2.2. Experiment to Measure the Coefficient of Adhesion of Mecanum Wheels by Tensile Method

2.2.1. Measurement methods

Based on the component P_ϑ, G_ϑ verified by (29), the following formula can be implied:

$$\vartheta = \frac{P_\vartheta}{G_\vartheta} \tag{32}$$

Table 2. Gradient angle and coefficient of adhesion on the wooden plane

Times	Adhesive coefficient	
	Vertical adhesive coefficient	Horizontal adhesive coefficient
1st time	0.165	0.215
2nd time	0.168	0.217
3rd time	0.167	0.216
4th time	0.166	0.213
5th time	0.164	0.215
Average	0.166	0.215

When a pulling force is applied tangentially to the vehicle F_k, if the traction force F_k is greater than or equal to the adhesion force (P_ϑ), the vehicle will be skidded.

$$F_\text{k} \geq P_\vartheta \tag{33}$$

In the braking scenario, the adhesive weight G_φ is determined by the vertical load acting on the braking wheels.

This experiment applies the tensile method to determine the tensile force (F_k) and vertical load acting on the braked wheels (G_ϑ), which calculates exactly the active wheel adhesion coefficient and the selected road surface.

2.2.2. Experiment equipment

The equipment for performing this experiment is spring dynamometer. It has a division of 0.1 N, the measuring range of the dynamometer is from 0 - 10 (N).

2.2.3. Experiment procedure

Experiment 1: Determine the traction coefficient when the vehicle is in longitudinal translational motion.

Step 1: Attach the dynamometer to the pre-mounted tow hook on the vehicle.

Step 2: Lock all wheels, put the car on a flat concrete road, gradually increase the vertical traction until the car starts to slide, record the value displayed on the dynamometer

Step 3: Repeat five times and finish the measurement.

Step 4: Then follow the same steps as above. We replace the concrete road surface with the road surface where the vehicle is applied, such as the wood floor surface and marble tile floor, and record the results in a number table.

Step 5: Calculate the value of the traction coefficient through traction force and grip weight.

Experiment 2: Determine the traction coefficient when the vehicle moves horizontally.

Step 1: Attach the dynamometer to the pre-mounted tow hook on the vehicle.

Step 2: Lock all wheels, put the car on a flat concrete surface, gradually increase the traction horizontally until the car starts to slide, record the value displayed on the dynamometer

Step 3: Repeat five times and finish the measurement.

Step 4: Calculate the value of the traction coefficient in the horizontal direction through traction force and grip weight.

2.2.4. Experiment results

Summarizing the experimental results from Table 3, we have the following Table 4.

Table 3. Pulling force when stretching the vehicle vertically and horizontally on concrete surfaces, wooden surfaces and marble surfaces.

Force	Surface	The vehicle moves vertically translational direction	The vehicle moves horizontally translational direction
Average traction (N)	concrete surface	5.42	6.2
	wooden surface	2.28	2.88
	marble surface	1.98	2.54

Table 4: Mecanum wheel's adhesion coefficient

	The vehicle moves vertically translational direction	The vehicle moves horizontally translational direction
Concrete surface	0.4	0.458
Wooden surface	0.169	0.213
Marble surface	0.146	0.188

Therefore, the result of Table 4 demonstrates some following points:

The Mecanum wheel's adhesive coefficient on marble surface has the smallest value. It has a higher value on wood, and reaches the highest value on concrete.

The coefficients of adhesion on the wood floor tested by the two methods are the same. Thus, the test results of both the drag and drop methods on the inclined plane are reliable.

When the vehicle moves on concrete roads, Mecanum wheels have an average adhesive coefficient of 0.4, which is smaller than regular wheels (0.76 -0.9). This result proves that the roller inclination angle of the wheel causes Mecanum wheels' adhesive coefficient to be smaller than that of regular wheels.

2.3. Experiment To Measure Rolling Friction Coefficient

2.3.1. Measurement methods

When the vehicle moves, its semi-dynamic recovery depends on the wheel's speed. So, the rolling friction coefficient f depends on the fourth order of the speed v. For simplicity, the coefficient of rolling friction is calculated depending on the first-order velocity function v:

$$f = K.v + F_0 \tag{34}$$

When the vehicle moves on a slope with an initial speed of zero, the air and engine resistances are negligible. The forces, including rolling resistance, gravity force, and slope resistance, influence the vehicle. Then, let the car drift on the level road. At the time of contact with the flat road, the car reaches the maximum speed and then slows down until it stops completely. At the height of H_1, H_2 and H_3, the car travels the distance on the slope S_{d1}, S_{d2}, and S_{d3}, then the vehicle moves on the road is equal to the distance respectively S_{n1}, S_{n2} and S_{n3} as shown in Fig. 4.

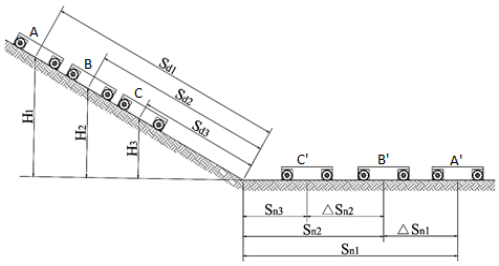

Fig. 4. Experiment of rolling friction coefficient

The force of inertia, resulting from the car's slow motion, acts as a traction force to propel the car forward. This force of inertia must be equal to or greater than the drag force. Therefore, to determine the car's rolling friction, we measure its inertia as it slows down, calculate the distance covered over the time it takes for the car to decelerate. At height H_1, the car covers the specific distance $S_{d1} + S_{n1}$ of the time t_1.

At height H_2, the car traveled the specific distance $S_{d2} + S_{n2}$ of the time t_2.

The time it takes for the car to travel the entire distance Δ is denoted as '*t*'. The average velocity over this segment, denoted as '*v*' is then calculated as follows:

So the time it takes for the car to travel the entire distance $\Delta S_{d1} + \Delta S_{n1}$ is: $\Delta t = t_2 - t_1$. The average velocity over this segment $A'B'$ is then:

$$\bar{v} = \frac{\Delta S_d + \Delta S_n}{\Delta t} \quad (35)$$

Considering the equation of conservation of energy, we obtain:

$$\Delta h = (f_0 + K.\bar{v}).\ Sin\ \alpha.\ \Delta S_d + (f_0 + K.\bar{v}).\ \Delta S_n \quad (36)$$

$$\Leftrightarrow \Delta h = f_0.\ Sin\ \alpha.\ \Delta S_d + f_0.\ \Delta S_n + K.\bar{v}.\ (\Delta S_d.\ Sin\ \alpha + \Delta S_n)$$

From the (36), determine these coefficients *K* and f_0. The relationship between rolling friction and speed can then be deduced as follows:

$$F_c = K.v + F_0 \quad (37)$$

2.3.2. Experimental equipment

Based on the main working environment of the vehicle, the experiment was carried out on concrete, marble, and wooden floors. Experimental equipment includes 3 parts as following:

- Spring dynamometer: The dynamometer has a division of 0.1 (N), the measuring range of the dynamometer is from 0 - 10 (N).
- Tape measure: The tape measure can measure up to 3 meters, the smallest measuring value is 1 millimeter.
- Stopwatch: Stopwatch can measure time in milliseconds and save the result.

2.3.3. Experiment sequence

The experiment is performed in 4 steps below:

1. Prepare a stopwatch.

2. Place the vehicle on the concrete surface, then attach the dynamometer tow hook to the top of the vehicle. Gradually increase traction until the vehicle rolls, and record the dynamometer value. Then find the coefficient F_0.

3. Put the car on the slope, connect the dynamometer to the hook towing the front of the car, and start pressing the clock; corresponding to this position, we have time $t_0 = 0$. Pull slowly and increase the force until the car starts to slide, determine the time t_1, s_1. Measure the distance s_1 and record the value of t_1 and s_1 in the data table from which the K-factor is calculated.

4. Repeat five times and finish the measurement.

Experimental sequence with wooden floor and marble tile floor as analogous to concrete floor, record the obtained results in the data table.

2.3.4. Experiment results

The experiment was conducted on the wooden surface, and the following results were obtained as described in Table 5.

Table 5. Distance and time measured on wooden surface

	Case 1		Case 2	
	h_1= 0.45		h_2= 0.51	
	S_d = 1.3		S_d = 1.5	
	S_{n1}	t_1	S_{n2}	t_2
1st time	6.18	4.55	6.49	4.87
2nd time	6.08	4,.32	6.54	4.89
3rd time	6.12	4.4	6.68	4.86
4th time	6.22	4,.72	6.55	5.2
5th time	6.1	4.46	6.66	4.98

Perform the same test steps on concrete and brick surfaces, then calculate the *F_0, K*, we get:

Table 6. Coefficients *F_0, K* on wooden surface, concrete surface, smooth brick surface.

Surface	F_0	K
Wooden surface	0.055	0.0201
Concrete surface	0.076	0.0419
Smooth brick surface	0.061	0.0376

Tables 6 show that the vehicle's rolling friction coefficient using Mecanum wheels on the wooden platform is the smallest, then on the brick and stone foundation, and finally, on the concrete foundation.

With the results of this experiment, the rolling friction was determined by (37), then the speed and motion trajectory of the AGV was simulated using Mecanum wheels with variable roller rotation angle.

Based on the differential equations (10), (27), and (28), we can determine the generalized coordinates of the AGV vehicle, then simulate the influence of the tilt angle roller shaft to traction force, rolling friction.

3. Effect of Roller Inclination Angle on Traction Force

With the characteristics of roller inclination angle, when applying torque evenly to all four wheels:

$M_1 = M_2 = M_3 = M_4 = 0.1$ (N.m), the vehicle moves in a reciprocating motion. In this case, the speed at the center of mass of the vehicle has only V_x component, V_y =0, as shown in Fig. 5.

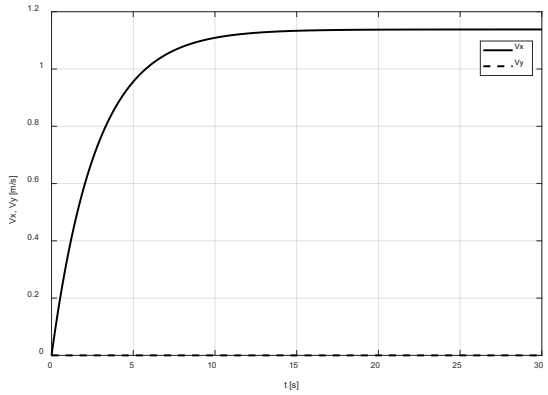

Fig. 5. V_x , V_y vehicle traveling in longitudinal translation

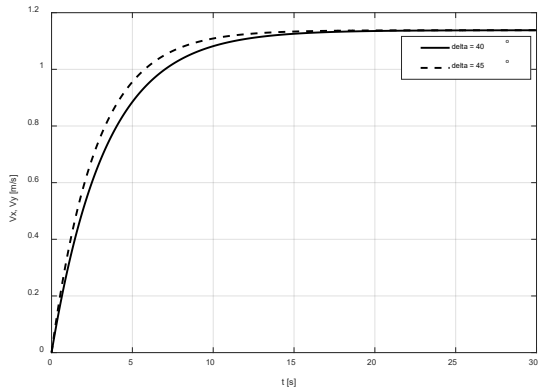

Fig. 6. Vehicle speed when changing angle

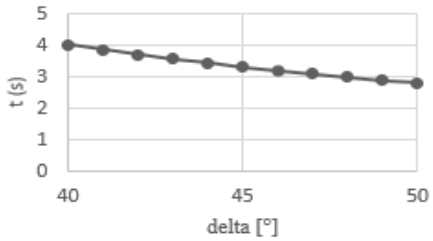

Fig. 7. Acceleration time when changing angle

Consider the vehicle traveling in longitudinal translation in the two cases of roller inclination angle $\delta = 40^0$ và $\delta = 45^0$.

From the result of Fig. 6, we can see that when changing the angle, the speed does not change but the vehicle's acceleration time is affected.

At time *t = 20(s)*, the car reaches the steady speed of $v_{max} = 1.17\ \left(\frac{m}{s}\right)$. When changing the angle of inclination of the roller, the time it takes the vehicle to reach the speed $v_1 = \frac{2}{3}$. v_{max}*= 0,78 (m/s),* changes as shown in Fig. 7.

So when the tilt angle δ increases, the time for the car to reach the speed v_1 = 0.78 (m/s) decreases. It follows that the car accelerates faster, which means the drag force of the vehicle increases as δ increases.

4. Fuzzy Logic Controller for AGV's Motion

The proposed fuzzy controller to control the vehicle movement direction has two inputs and four outputs, specifically as follows:

The two inputs are deviation Error and deviation rate *d_Error* (differential of error). The outputs are the active torque increments applied to the front left, right front, rear left, and rear right wheels, respectively (denoted *as d-FL, d-FR, d-RL, d-RR* in Fig. 8).

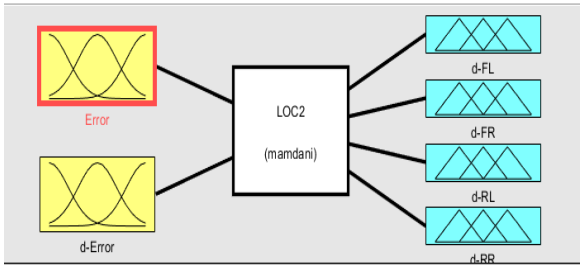

Fig. 8. Fuzzy Calculator

The inputs are fuzzy to 8 values: No skew (*KL*), little left skew (*LTI*), much-left skew (*LTN*), little right skew (*LPI*), much right skew (*LPN*), negative value (*N*), zero value (*Z*), positive value (*P*) (Fig. 9, Fig. 10).

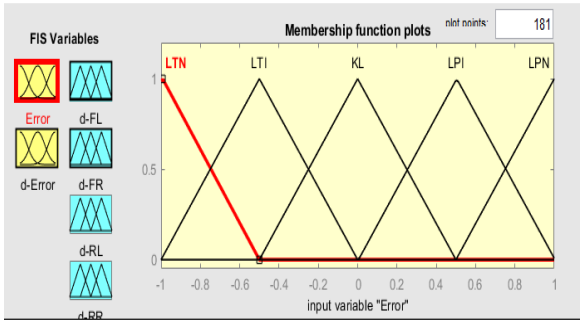

Fig. 9. Input error fuzzification

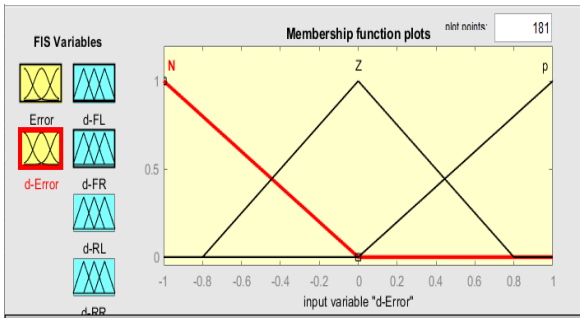

Fig. 10. Input differential fuzzification

The output parameters are dimmed into 7 values, respectively: large negative (*NL*), medium negative (*NM*), small negative (*NS*), zero (*Z*), small positive

(*PS*), medium positive (*PM*) and large positive (*PL*) (Fig. 11).

The control law is built on the principle that the larger the deviation, the larger the control effect, and the larger the deviation derivative, the larger the control effect. The control laws are presented in Table 7.

Table 7. Fuzzy controller rules

error / d_error	LTN	LTI	KL	LPI	LPN
N	PL	PM	PS	Z	NS
Z	PM	PS	Z	NS	NM
P	PS	Z	NS	NM	NL

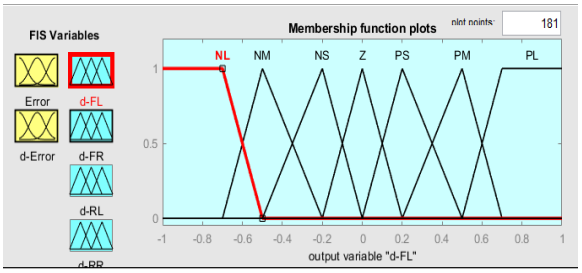

Fig. 11. Output parameter fuzzification

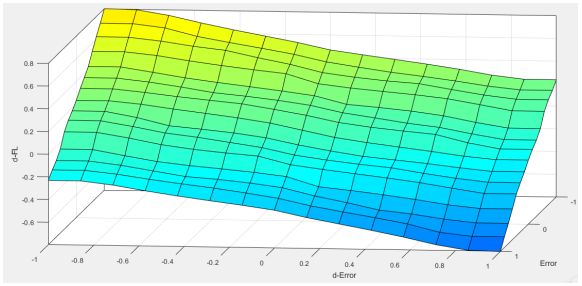

Fig. 12. Graph of input and output characteristics of fuzzy controller

With the rules, the input and output parameters are set, and the quantitative relationship between the inputs and outputs is established, as shown in Fig. 12.

Apply a fuzzy controller to control the vehicle to move along a sinusoidal trajectory and we obtain simulation results and the vehicle's motion trajectory is very close to the desired motion trajectory (Fig. 13).

From the above firgure, it can be seen that the desired and simulated trajectory deviation is very small, which proves that the fuzzy controller has achieved a relatively high level of accuracy in controlling the vehicle movement and reducing the error number during control.

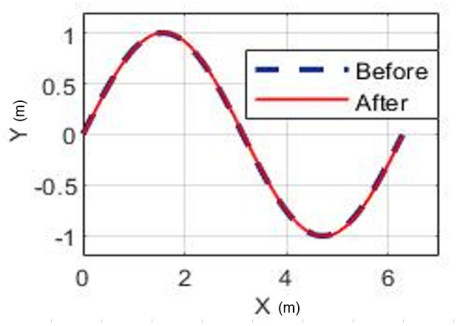

Fig. 13. Motion trajectory control results

5. Conclusion

This paper presents many methods to measure the coefficient of cohesion and the coefficient of rolling resistance on platforms such as concrete, wood, brick, and stone. Since then, we have established the equation of motion of the AGV, which uses the Mecanum wheel with a variable roller inclination angle. Simulation results show that when the tilt angle of the roller increases, the traction force increases, increasing the vehicle's acceleration. However, the rolling resistance also increases, adversely affecting the vehicle's performance. The fuzzy control method has been applied to control the vehicle's motion trajectory. The simulation results have confirmed that the fuzzy controller effectively ensures the vehicle's desired motion trajectory.

References

[1] Tran Dinh Phuc, Research on Mecanum wheel design for forklift trucks, M.S. thesis, Ho Chi Minh City University of Technology, 2012.

[2] Vo Phong Thien, Design of a self-propelled robot that tracks activities in the factory, M.S. thesis, Ho Chi Minh City University of Technology 2017.

[3] Florentina Adascalitei, Ioan Doroftei, Practical applications for mobile robots based on Mecanum wheels, The Romanian Review Precision Mechanics, Optics & Mechatronics, No. 40, 2011.

[4] Felix Becker, B. Adamov, I. Zeidis, K. Zimmermann, An approach to the kinematics and dynamics of a four-wheeled mecanum vehicles, Scientific journal of IFTOMM Problems of Mechanics no 2(55), International conference mechanics, 2014.

[5] Z. Hendzel and L. Rykała, Modelling of dynamics of a wheeled mobile robot with mecanum wheels with the use of lagrange equations of the second kind, Int. J. of Applied Mechanics and Engineering, vol.22, No.1, pp.81-99, 2017. https://doi.org/10.1515/ijame-2017-0005

[6] Matthieu Lamy, Mechanical development of an automated guided vehicle, M.S. Thesis, KTH Industrial Engineering and Management Machine Design, 10-10-2016.

[7] P. L.Sarode, Design and fabrication of forklift with multi-directional wheel, International Journal of

Innovative Research in Science, Engineering and Technology, Vol. 8, Issue 4, 2019, https://doi.org/10.15680/IJIRSET.2019.0804091

[8] Sonawane, Nishant, An experimental method to calculate coefficient of friction in mecanum wheel rollers and cost Analysis Using DFMA Techniques, Dissertations and Theses, Embry-Riddle Aeronautical University, 2015.

[9] Zeidis, Igor Zimmermann, Klaus, Dynamics of a four-wheeled mobile robot with Mecanum wheels, Journal of Applied Mathematics and Mechanics, ISSN 1521-4001, 2019, https://doi.org/10.1002/zamm.201900173.